Velocity dependence of KLL Auger emission from hollow atoms formed during collisions of hydrogenic N^{6+} ions on surfaces

J. Limburg, S. Schippers, I. Hughes, R. Hoekstra, and R. Morgenstern
Kernfysisch Versneller Institute, Zernikelaan 25, 9747 AA Groningen, The Netherlands

S. Hustedt, N. Hatke, and W. Heiland
Universität Osnabrück, D-49069 Osnabrück, Germany
(Received 21 November 1994)

This paper presents a detailed description of KLL Auger spectra arising from collisions of hydrogenic N^{6+} ions on clean Si(100) and Al(110) surfaces at energies ranging from 78 eV up to 60 keV and at incident angles from 2.5° up to 45°. Atomic structure calculations of KLL Auger energies and decay rates for hollow atoms, together with simulations of the projectile trajectories, support a model in which the de-excitation of the ions proceeds essentially via two mechanisms. Before the ion enters the "close collision range," a few of its L-shell vacancies are filled by Auger cascades involving outer shell electrons. But as soon as the projectile suffers close collisions, L-shell vacancies are rapidly filled by direct capture of target core electrons. The time scale of the latter mechanism is determined by the collision frequency.

PACS number(s): 79.20.Nc, 31.15.−p, 34.90.+q, 32.10.−f

I. INTRODUCTION

Neutralization of highly charged ions (HCI) at solid state surfaces is accompanied by the emission of a large number of electrons. A study of the energy and angular distributions of these electrons provides detailed insight into the neutralization dynamics. Previous studies have led to a coherent model describing the interaction of HCI with surfaces. In this model, a HCI approaching a surface is neutralized well in front of the surface by electron capture into high-Rydberg states, forming a hollow atom [1–4], i.e., an atom in a highly excited state where only outer shells are populated whereas inner shells are almost empty.

Heading towards the surface, the projectile subsequently starts to deexcite. Whether or not the projectile will deexcite to its ground state before it hits the surface depends on the deexcitation time scales and on its velocity component $v_\perp$ perpendicular to the surface. In general the time the projectile spends above the surface is by far too short to allow for a complete deexcitation. Therefore, a large fraction of the inner shell vacancies will only be filled after the projectile has suffered close collisions with one or more surface atoms. Consequently, Auger electron spectra contain information on both "above" [1,3,5] and "below" [6–10] surface emission.

However, until now, not much attention has been paid to the question how the component of the projectile velocity *parallel* ($v_\parallel$) to the surface affects the electron emission dynamics. Both $v_\perp$ and $v_\parallel$ determine whether the projectile enters the surface or is reflected. The relaxation of reflected hollow atoms can be observed for periods of time orders of magnitude larger than for atoms entering the target since projectile electrons and photons cannot escape the solid beyond a certain escape depth.

In this paper we present general concepts that allow for an explanation of the main features of the KLL Auger spectra obtained from the neutralization of hydrogenic ions at various solid surfaces. Using these concepts we discuss KLL spectra resulting from collisions of N^{6+} on Al(110) and Si(100), taken at different projectile energies E_0 and incident angles ψ.

II. EXPERIMENT

The N^{6+} ions were extracted from the KVI electron cyclotron resonance (ECR) ion source, ECRIS-2 [11]. After charge selection and focusing, the beam enters an ultrahigh vacuum μ-metal collision chamber (base pressure below 2×10^{-8} Pa) through a set of 2-mm-diameter diaphragms. Low-energy primary beams are produced by floating the complete setup on source potential V_{ECR} minus an offset voltage V_Δ in series. Thus the final beam energy E_0 is not influenced by variations in V_{ECR}. Measurements of beam energies have shown the existence of a "plasma voltage" ΔV of (13 ± 2) V. This residual energy is caused by the plasma potential of the ECR source and depends only slightly on the source settings. All beam energies E_0 given in this paper are calculated by $q(V_\Delta + \Delta V)$ eV.

The targets used in the experiments were Al(110) and B-doped, p-conducting Si(100) crystals. Before each experiment, the targets were sputter cleaned with 3.0-keV Ne^{3+} ion beams at 5° incidence to the surface and annealed. Surface quality was monitored with low-energy ion scattering methods [12].

The electron spectra were measured with a 180° spherical electrostatic analyzer which can be rotated between $\theta = 0°$ and $\theta = 140°$ with respect to the primary beam direction. The energy resolution of the analyzer is $5 \times 10^{-3}E$ full width at half maximum (FWHM) and

its acceptance at the center of the target is $11.2 \times 10^{-8}E$ (sr eV), with E the energy of the detected electrons. The minimum width of the analyzer spot on target is about 3.5 mm. A detailed description of the energy calibration of the analyzer is presented elsewhere [13].

III. RESULTS

Figures 1 and 2 are plots of the KLL Auger spectra arising from the interaction of N^{6+} ions with Si(100) and Al(110) surfaces. A random azimuthal angle and the $1\bar{1}0$ surface direction have been chosen, respectively. The spectra in Figs. 1 and 2 have been corrected for analyzer transmission. No background subtraction has been applied. Incident angle ψ and primary beam energy E_0 have been varied simultaneously such that $v_\perp$ was kept constant. First of all, it should be noted that in the spectra obtained from both the Al(110) and Si(100) targets with increasing $v_\parallel$ a very sharp peak shows up at the high-energy side (383 eV) of the KLL spectrum. Furthermore, in both series, the intensity of the peak at the low-energy side (at 347 eV in Si and 350 eV in Al) does not change considerably over the indicated (ψ, E_0) range. But the intensity of this peak is target dependent since it is more pronounced for the Si target.

Figure 3 presents spectra taken under specular reflection conditions, varying the parallel velocity $v_\parallel$ by a factor of 20. These velocities correspond to average interatomic $1\bar{1}0$ traveling times, i.e., the time needed to travel along the $1\bar{1}0$ direction between adjacent target atoms, ranging from 0.3 fs (60 keV) to 7 fs (150 eV). The velocity component perpendicular to the surface $v_\perp$ varies by a factor of 8 since this velocity is determined by the sum of the beam energy perpendicular to the surface (30 eV at 16 keV) plus the energy gain due to image charge acceleration ($\simeq$ 15 eV) [4,14–16]. This series shows a shift of intensity towards higher electron energies for increasing projectile energy.

In Figs. 4(a) and 4(b), we plotted the measured Doppler shift of the two sharp peaks for the Al target. The plotted points are measurements, the lines are calculated assuming electron emission on the ingoing path (solid line) and on the reflected path (dotted line). The Doppler shifts were measured with $\psi = 2.5°$ and $E_0 = 16$ keV.

IV. ION TRAJECTORY SIMULATIONS

In order to get an insight into the in-depth ion distribution at the instant of KLL electron emission and into the traveling paths of the projectiles during their interaction with the solid, we performed Monte Carlo ion trajectory simulations using the MARLOWE computer code [18]. Using this code and additional routines we are able to simulate and visualize the trajectories followed by the projectiles for the ψ, E_0 combinations as depicted in Figs. 2 and 3. The MARLOWE program simulates the trajectories followed by the projectiles in a binary collision approximation; between collisions, particles move in straight lines. The interatomic potential is modeled according to Ziegler *et al.* [19]. The surface is implemented as a perfect Al(110) surface, oriented in the $1\bar{1}0$ channeling direction. Thermal lattice vibrations are accounted for by the Debye model with a Debye temperature of 400 K. A kinetic energy gain perpendicular to the surface of 15 eV due to image charge acceleration is also accounted for.

The results of the simulations are shown in Figs. 5 and 6. In Fig. 5 collision conditions as in the spectra of Fig. 2 were chosen, i.e., varying ψ and E_0 such that $v_\perp$ is constant. The simulations show that nearly all primary particles are reflected from the first few target layers for incident energies from 4 keV down to 450 eV. For even lower energies such as 120 and 78 eV, a large part of the beam will be stopped in the first few layers of the target. Second, the number of close collisions with target atoms varies significantly over the indicated ψ, E_0 range. In the present context close collisions are defined

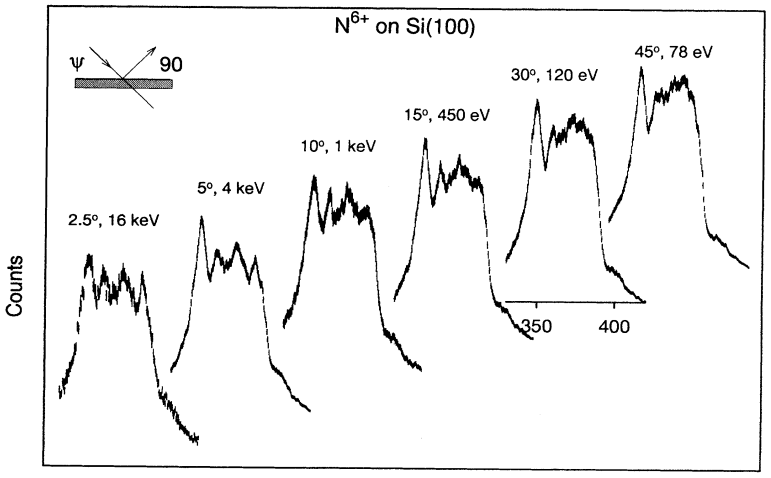

FIG. 1. KLL Auger spectra of N^{6+} ions on Si(100). The beam energy E_0 and incident angle ψ have been changed in order to keep $v_\perp$ constant.

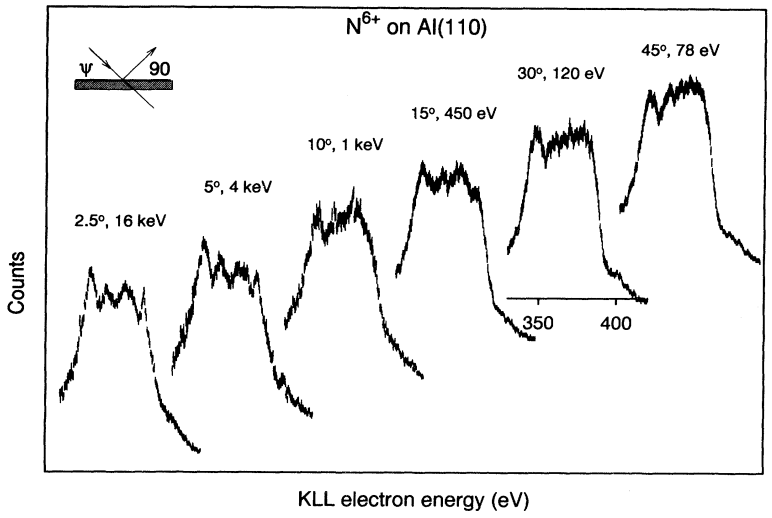

FIG. 2. KLL Auger spectra of N^{6+} on Al(110). E_0 and ψ same as in Fig. 1.

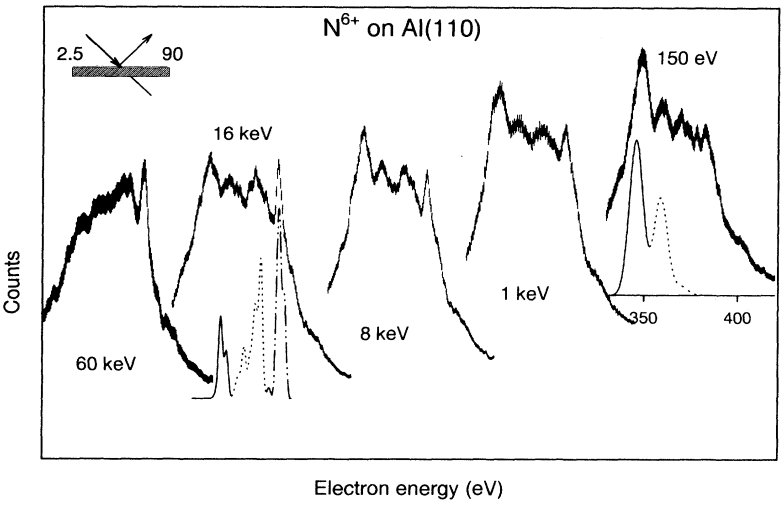

FIG. 3. Auger spectra of N^{6+} ions on Al(110). All spectra are taken under specular reflection conditions, the velocity parallel to the surface ($v_{||}$) changes a factor of 20. The lines are simulated spectra, in the 150-eV spectrum $1s\,2s^2/2s2p\,3l^4$ states are assumed, in the 16-KeV spectrum a $1s(2s^2 2p^4)^3P$ state has been taken. The spectra are calculated according to algorithms described by Schippers [21]. KL_1L_1, $KL_1L_{2,3}$, and $KL_{2,3}L_{2,3}$ decay is depicted by straight, dotted, and straight-dot-dot lines, respectively

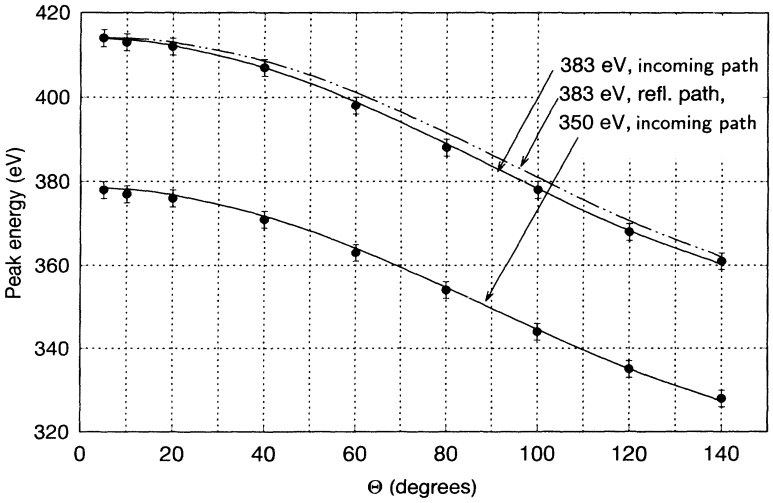

FIG. 4. Doppler shifts of 350-eV and 383-eV peaks and of FWHM, measured for different angles of observation (Θ) using 16-keV N^{6+}, $\psi = 2.5$ on Al(110). Solid lines are calculated shifts assuming emission on the ingoing path, dotted line on the reflected path.

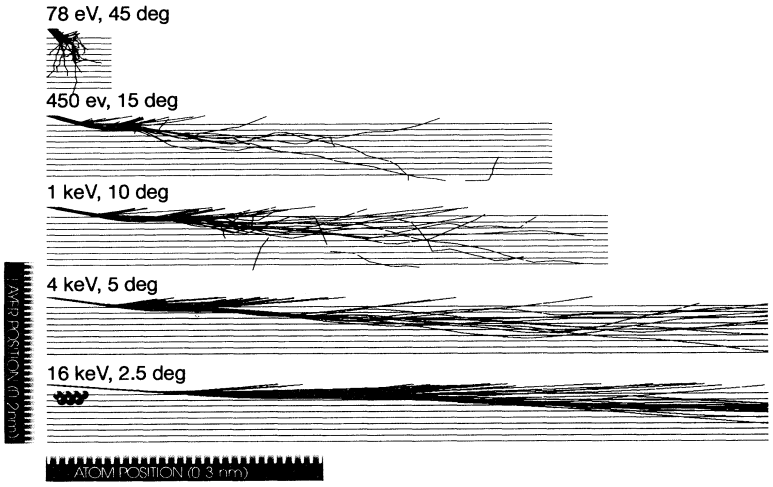

FIG. 5. Ion trajectories simulated using MARLOWE. In these simulations the same ψ, E_0 parameters as in Figs. 1 and 2 were chosen. The dotted lines are the target layers, the position of the atoms is shown below. The units are in lattice constants ($a = 0.405$ nm).

as collisions with an impact parameter smaller than the projectile L-shell radius (see below). In case of 16-keV projectiles, a few tens of close collisions occur, whereas in the case of low energies such as 120 and 78 eV only one or two close collisions per incident ion are encountered. Furthermore, it is seen that high-energy projectiles travel for a relatively long time (10–100 fs) on their incident trajectory or parallel to the target surface.

In Fig. 6 we show the trajectories calculated using the same ψ, E_0 as in Fig. 3. Now only for 16- and 60-keV beams some penetration into the bulk material occurs. In this case the incident ions are seen to travel parallel to the surface, sometimes several layers deep inside the solid. At all other energies, the projectiles are reflected by the first or second layer of the target surface. Therefore, energy losses due to inelastic scattering of electrons emitted inside the solid will be minimal in all KLL Auger spectra presented in this article, except for the 2.5°, 60-keV spectrum. Furthermore, it is seen that again the average number of close collisions undergone by the projectiles dramatically decreases with decreasing energy. For low projectile energies, the image charge acceleration of the projectiles towards the target significantly increases the incident angle ψ (even up to 20° for a 2.5°, 150-eV beam). This increase alters the collision dynamics such that particles more easily penetrate the bulk and are stopped after a few collisions.

Table I lists the percentage of reflected projectiles, their flight time along the surface, the average number of collisions undergone and the percentage of collisions with impact parameters smaller than 2 a.u. These numbers result from simulations of trajectories of 5×10^4 projectiles incident on the Al(110) surface using $\psi = 2.5$ and various energies. The large uncertainties in the average numbers of collisions are due to the particles that channel along the $[1\bar{1}0]$ surface directions. After listed flight times 95% of the reflected projectiles have left the surface. Conclusively, the simulations show that under

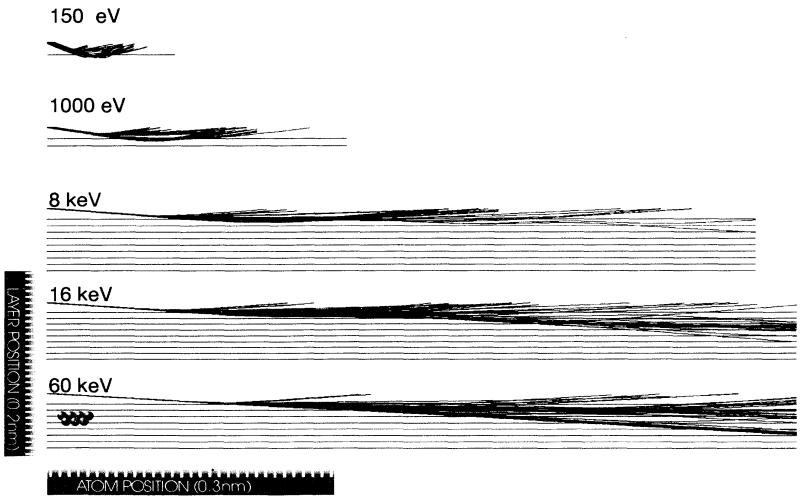

FIG. 6. Ion trajectories simulated using MARLOWE. In these simulations the same ψ, E_0 parameters as in Fig. 3 were chosen. Note the penetration occuring for 60-keV projectiles, in all other cases, the projectiles are reflected on the first or second target layers.

TABLE I. Reflected projectiles, flight times, mean number of collisions and the precentage of these collisions with impact parameters smaller than 2 a.u. for different energies. The flight time of the projectiles is the time after which 95% of the reflected particles have left the surface. The large uncertainties in the numbers of collisions is due to particle channeling along $1\bar{1}0$ channels.

E_0 (keV)	Reflection (%)	T (fs)	No. coll	No. coll ($d < 2$ a.u.) (%)
0.15	99.9	40	10± 4	≤ 1
1.0	99.8	50	30± 10	5
8.0	99.7	60	80± 20	11
16.0	95.0	200	500± 100	13
64.0	79.0	400	1400± 300	50

the present experimental conditions no significant bulk penetration occurs. Consequently, the electron spectra are merely disturbed by solid state effects.

V. MODELING *KLL* AUGER EMISSION

In the previous section the effects of the projectile trajectories at or inside the solid on the KLL Auger electron emission distribution are discussed. It is clear that the point of emission, at or inside the solid, determines the elastic and inelastic electron energy losses and thereby part of the shape of the KLL Auger structure. But the typical electron emission time scales, determined by both the KLL Auger decay rates and the L-shell filling rates, not only give the in-depth emission distribution but also the distribution of configurations present at the moment of KLL decay. It is evident that the ratio of the KLL decay rate, Γ_K and the L-shell filling rate Γ_L determines whether KLL decay occurs preferably with a small or large number of L electrons present. It has been shown by means of atomic structure calculations that with increasing number of L electrons KLL Auger energies shift to higher values [8,17,20]. Accordingly an analysis of the measured K Auger energy distribution allows a determination of the projectile state at the instant of K Auger emission.

In this section a simple model will be presented in which the probability that a certain number of L electrons is captured before KLL decay occurs, is calculated. The KLL Auger line intensity $I_{if}(r)$ resulting from a transition from an initial state i with r L electrons to a final state f with $r-2$ electrons is given by its initial population n_i times the branching ratio $\Gamma_{if}(r)/\sum_f \Gamma_{if}(r)$. However, to arrive at the experimentally observed intensity, we have to incorporate (i) the *probability* $P_K^\gamma(r)$ that r L electrons are actually present and (ii) a time window P_T reflecting the limited observation time in case the projectiles penetrate into the solid from where electrons cannot be observed beyond a certain escape depth. Therefore, we have

$$I_{if}(r) = C n_i \frac{\Gamma_{if}(r)}{\sum_f \Gamma_{if}(r)} P_K^\gamma(r) P_T \qquad (1)$$

in which C is a calibration constant.

The concept of a limited time window, denoted by P_T, has been discussed in detail by Schippers *et al.* [21]. In the experiments under consideration here, no significant penetration of the solid occurs. Therefore, the time window is roughly given by the width of the spectrometer spot on the target divided by the parallel velocity of the projectiles, a number in the order of ns in case of 60-keV projectiles. Since most Auger transitions are much faster than that, the time window factor P_T in practice equals one.

Atomic structure calculations

In order to identify the transitions that contribute to the sharp peaks we observe in the nitrogen KLL Auger spectra, we calculated the energies and rates for all states present within the configurations $1s\,2l^r\,3l^{6-r}$ with $2 \leq r \leq 6$ using the Hartree-Fock atomic structure computer code by Cowan [22]. It should be noted here that similar calculations have been presented earlier by Hansen *et al.* [20]. Our calculations are similar to theirs but do distinguish decay towards distinct final states which are actually resolved in the spectra (see, e.g., Refs. [23,24,21]).

Not all states present within the mentioned configurations will actually contribute to the KLL Auger spectrum. Coster-Kronig (CK) transitions redistribute the L electrons, yielding "final" states with maximum binding energies [24,21]. KLL transition rates Γ_K are 10 to 100 times smaller than the competing Coster-Kronig rates Γ_{CK} [21]. Recently, Diez Muiño *et al.* [25] presented calculations of Coster-Kronig rates inside a free electron gas yielding roughly the same numbers. Therefore, the resulting KLL Auger spectrum mainly arises from the decay of the Coster-Kronig "final" states.

Table II lists the rates and Auger energies of all states remaining after this Coster-Kronig redistribution, decaying via KL_1L_1, $KL_1L_{2,3}$, or $KL_{2,3}L_{2,3}$ Auger transitions for different numbers of L electrons r. In this notation L_1 stands for a $2s$ electron and $L_{2,3}$ for $2p$ electrons participating in the Auger transition [26]. The various decay channels in general have different rates and Auger energies. For a given r, the KL_1L_1; $KL_1L_{2,3}$; $KL_{2,3}L_{2,3}$ subgroups are well separated in energy and lead to different peaks that can be well resolved by our spectrometer. A more detailed assignment of peaks, possible for the case $r = 2$ [21], is prohibitive in general because of the large number of transitions involved for $r \geq 3$. Therefore, the energies and rates given in Table II are mean values averaged over all transitions within a given subgroup $\gamma \in \{KL_1L_1;\ KL_1L_{2,3};\ KL_{2,3}L_{2,3}\}$,

$$\overline{E}^\gamma(r) = \frac{\sum_i n_i E_i^\gamma(r)}{\sum_i n_i} \qquad (2)$$

and

$$\overline{\Gamma}^\gamma(r) = \frac{\sum_i n_i \Gamma_i^\gamma(r)}{\sum_i n_i} \,. \qquad (3)$$

A statistical population $n_i = 2J_i + 1$ of all states has

been assumed throughout, with J_i being the total angular momentum of state i. Coster-Kronig redistribution has been accounted for.

In Fig. 7(a) the calculated subgroup specific average energies are plotted as a function of the number r of L electrons. Evidently $\overline{E}^{\gamma}(r)$ increases with increasing r. Moreover we find that both KL_1L_1 and $KL_{2,3}L_{2,3}$ subgroups are rather sharply peaked in contrast to the $KL_1L_{2,3}$ subgroup which for $r > 3$ covers a broad range of Auger energies in between the KL_1L_1 and the $KL_{2,3}L_{2,3}$ peaks.

Figure 7(b) displays the behavior of $\overline{\Gamma}^{\gamma}(r)$ versus r. For the cases $r = 2, 3$ $KL_{2,3}L_{2,3}$ rates have been omitted since the corresponding $1s\,2p^2\,3l^4$ and $1s\,2s2p^2\,3l^3$ configurations primarily decay by Coster-Kronig transitions [24,21]. Figure 7(b) shows that $\overline{\Gamma}^{KL_1L_1}$ rapidly decreases with r while $\overline{\Gamma}^{KL_1L_{2,3}}$ and $\overline{\Gamma}^{KL_{2,3}L_{2,3}}$ significantly increase. Furthermore, for small r KL_1L_1 decay dominates but for larger r $KL_1L_{2,3}$ and $KL_{2,3}L_{2,3}$ transitions are faster.

TABLE II. N^{6+} hollow atom configurations, transition rates and energies for 2 up to 6 L electrons (r) (rates Γ are in units of s^{-1}; energies are in eV). The remaining electrons are taken in the M shell. The energies $E_{KL_1L_{2,3}}$ are averages for 4, 5, and 6 L electrons, see text. Numbers in parentheses denote powers of 10.

r	State	$\Gamma_{KL_1L_1}$ $E_{KL_1L_1}$	$\Gamma_{KL_1L_{2,3}}$ $E_{KL_1L_{2,3}}$	$\Gamma_{KL_{2,3}L_{2,3}}$ $E_{KL_{2,3}L_{2,3}}$
2	$1s\,(2s^2\,{}^1S)^2S$	9.6 (13)		
		347		
	$1s\,(2s2p\,{}^3P)^4P$		1 (8)	
			352	
	$1s\,(2s2p\,{}^3P)^2P$		8.8 (12)	
			358	
3	$1s\,(2s^22p\,{}^2P)^3P$	7.4 (13)	3.6 (13)	
		347	358	
	$1s\,(2s^22p\,{}^2P)^1P$	7.4 (13)	1.2 (11)	
		350	360	
	$1s\,(2s2p^2\,{}^4P)^5P$		1 (7)	1 (9)
			349	360
	$1s\,(2s2p^2\,{}^4P)^3P$		1.9 (13)	1 (9)
			358	368
4	$1s\,(2s^22p^2\,{}^1S)^2S$	7.7 (13)	4.2 (13)	2.7 (13)
		346	362	377
	$1s\,(2s^22p^2\,{}^1D)^2D$	5.5 (13)	4.5 (13)	6.8 (13)
		349	360	375
	$1s\,(2s^22p^2\,{}^3P)^4P$	5.3 (13)	6.0 (13)	6.3 (8)
		347	362	371
	$1s\,(2s^22p^2\,{}^3P)^2P$	5.3 (13)	6.0 (13)	4 (9)
		352	358	375
	$1s\,(2s2p^3\,{}^5S)^6S$		3 (7)	3 (8)
			357	370
	$1s\,(2s2p^3\,{}^5S)^4S$		2 (13)	1 (9)
			357	371
5	$1s\,(2s^22p^3\,{}^4S)^5S$	3.6 (13)	4.2 (13)	6.7 (8)
		352	364	373
	$1s\,(2s^22p^3\,{}^4S)^3S$	3.6 (13)	5.1 (13)	9 (9)
		354	366	371
	$1s\,(2s^22p^3\,{}^2P)^3P$	5.0 (13)	7.5 (13)	5.4 (13)
		350	365	380
	$1s\,(2s^22p^3\,{}^2P)^1P$	5.2 (13)	5.8 (13)	5.4 (13)
		353	367	383
	$1s\,(2s^22p^3\,{}^2D)^3D$	3.6 (13)	7.6 (13)	7.6 (13)
		352	365	378
	$1s\,(2s^22p^3\,{}^2D)^1D$	3.6 (13)	5.1 (13)	7.6 (13)
		352	368	378
6	$1s\,(2s^22p^4\,{}^1S)^2S$	5.0 (13)	9.9 (13)	7.5 (13)
		353	370	384
	$1s\,(2s^22p^4\,{}^3P)^4P$	3.0 (13)	8.8 (13)	6.5 (13)
		354	369	383
	$1s\,(2s^22p^4\,{}^3P)^2P$	3.0 (13)	5.8 (13)	6.5 (13)
		357	369	386
	$1s\,(2s^22p^4\,{}^1D)^2D$	3.0 (13)	5.3 (13)	6.5 (13)
		357	367	386

A stepwise L-shell filling model

The number of L electrons present before KLL decay occurs depends on the outcome of the competition between KLL decay (rate Γ_K) and L-shell filling (rate Γ_L). For a rapid L-shell filling ($\Gamma_L \gg \Gamma_K$) KLL decay will predominantly occur after the L shell is filled up to its maximum. For slow L-shell filling, KLL Auger decay occurs mainly as soon as a second L electron is present.

In order to quantify the competition between KLL Auger processes and L-shell filling we calculate the probability of KLL Auger emission from a configuration containing r L electrons as

$$P_K(r) = \frac{\Gamma_K(r)}{\Gamma_L(r)+\Gamma_K(r)} \prod_{i=0}^{r-1} \frac{\Gamma_L(i)}{\Gamma_L(i)+\Gamma_K(i)} , \qquad (4)$$

where the first factor is the branching ratio for KLL Auger decay of a configuration containing r L electrons and the product is the probability that r electrons are present before KLL Auger decay occurs. From $P_K(r)$ a subgroup specific probability is calculated by multiplying with the corresponding branching ratio, i.e.,

$$P_K^{\gamma}(r) = P_K(r)\frac{\overline{\Gamma}_K^{\gamma}(r)}{\Gamma_K(r)} . \qquad (5)$$

For $r \geq 2$, the mean KLL Auger rate for initial configurations containing r electrons $\Gamma_K(r)$, is calculated as the sum of the subgroup specific KLL Auger rates plotted in Fig. 7(b). For $r < 2$ this rate is taken to be zero. $\Gamma_L(r)$ denotes the rate for adding an L electron when r electrons are already present. We distinguish two mechanisms filling the projectile L shell, namely L Auger processes and direct capture of target electrons. While the former is taken to be velocity independent the latter is taken to be proportional to the number of close collisions with target electrons. We, therefore, write

$$\Gamma_L(r) = \Gamma_L^A(r) + P_L(r)\frac{v}{d} , \qquad (6)$$

where $\Gamma_L^A(r)$ denotes the rate for L Auger processes and d is the distance between neighboring target atoms in

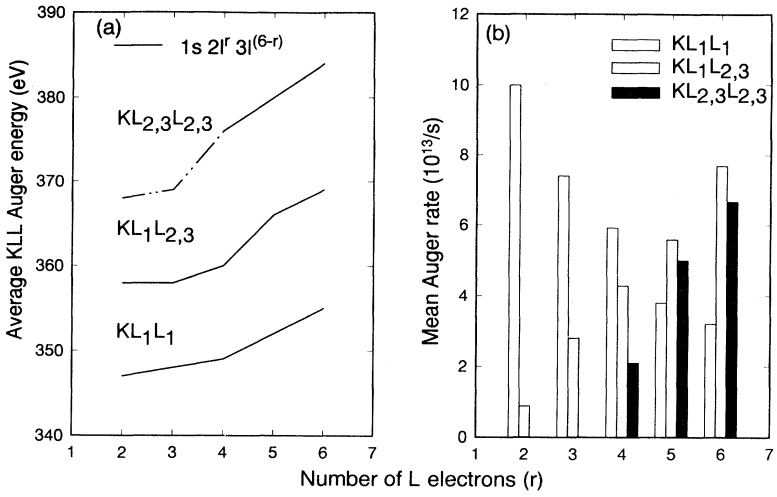

FIG. 7. Calculated sublevel specific Auger energies (a) and lifetimes (b) of hollow atom states present at the moment of KLL decay, as a function of the number of L electrons.

the direction of the projectile velocity v. $P_L(r)$ denotes the probability of actually transferring an electron from a target atom to the projectile L shell during a close collision event. It should be noted that a similar approach was presented by Köhrbrück *et al.* [28], and by Page *et al.* [29].

Figure 8 shows plots of $P_K^\gamma(r)$ for projectile energies of 150 eV, 8 keV, and 60 keV, respectively. This figure reveals that for high energies nearly all KLL emission occurs after the L shell has been filled up to its maximum and mainly involves $KL_1L_{2,3}$ and $KL_{2,3}L_{2,3}$ combinations. This results in contributions to the high-energy side of the spectrum, and, most prominently, to the 383-eV peak (see Table II). For low energies a major fraction of the emission is from a $1s\,2s^2\,3l^4$ state contributing to the low-energy peak at 350 eV. For projectile energies between 150 eV and 60 keV a fraction of 70 up to 80 percent of the KLL emission occurs from the "extreme" configurations with $r = 2$ and $r = 6$. The emission from the "in between" configurations with $3 \leq r \leq 5$ plays a minor role; at all energies used the KLL spectrum mainly consists of a mixture of electrons emitted from configurations with $r = 2$ and $r = 6$.

In the simulations depicted in Fig. 8, the capture probability P_L has been taken equal to $(8 - r)/16$, i.e., to at most $1/2$ when the L shell is still empty. Values for the L Auger filling rate $\Gamma_L^A(r)$ have been taken from recent work by Diez Muiño *et al.* [25] who calculated Auger rates for projectiles located inside an electron gas with an Al electronic density. Since under the experimental conditions here, all processes occur very close to the target surface, i.e., at distances at which the electronic density approaches the bulk values, the use of the calculated rates [25] is justified. These calculations show a strong, almost exponential increase in LVV rates with decreasing effective charge (i.e., increasing r), from about 5×10^{13}/s for $r = 0$ to about 1.5×10^{15} for $r = 5$. This implies that even for 60 keV projectiles ($v/d \simeq 3 \times 10^{15}$/s), both direct filling and Auger filling play an important role for large r. On the other hand, for small r, $\Gamma_L(r)$ is mainly given by the second, projectile velocity dependent term in Eq. (6).

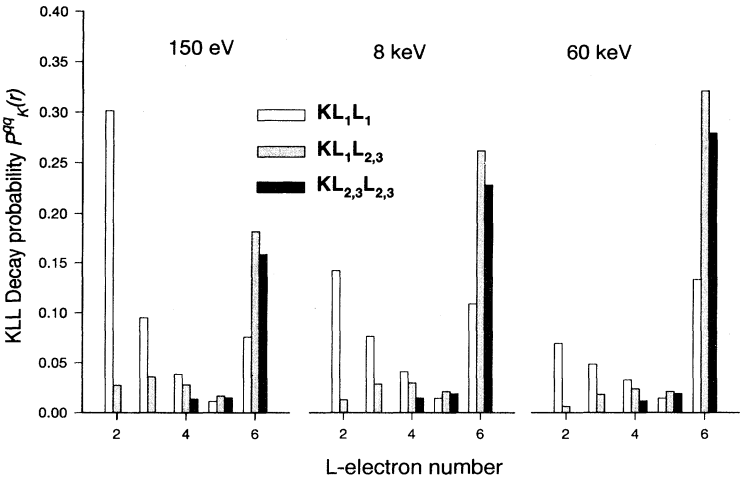

FIG. 8. Calculated KLL emission probability P_K^γ for 2 up to 6 L electrons as a function of beam energy.

The exact nature of the L-shell filling during binary collisions is not well known. An efficient Landau-Zener type of quasiresonant charge transfer between the projectile K shell and inner target shells during close collisions with target atoms has been reported earlier by Schippers *et al.* [9]. A comparable type of transfer between the Al and Si $2p$ core levels (binding energies 80 eV, and 100 eV, respectively) and the nitrogen L levels (ranging in binding energy from about 80 eV for a $1s\,3l^6$ configuration to about 20 eV for a $1s\,2l^5\,3l$ configuration) might be responsible for the direct filling described above. A straightforward application of the mentioned Landau-Zener model results in a decreasing exchange probability with increasing separation of projectile and target levels, i.e., with increasing L occupancy. Moreover, projectile-target distances at which level crossings occur are smaller than 1 a.u. Our trajectory simulations indicate however that such close collisions are rare for grazingly incident keV projectiles.

Recently, Burgdörfer *et al.* [30] presented simulations of the neutralization and deexcitation of O^{q+} ions in grazing incidence with a Au(110) surface as observed by Folkerts *et al.* [31]. Based on a modified version of the "over-barrier" model [4] including dynamical screening of the projectile levels by target electrons, a very efficient filling of L vacancies by quasiresonant target core electrons is found. The distances at which this type of exchange occurs are in the order of one to few a.u. In our experiments discussed here, this condition is fullfilled for a few (150-eV projectiles) up to tens (16-keV projectiles) of consecutive collisions, as can be inferred from Table II and Fig. 6.

However, until now it is not clear how many electrons are actually captured during a single binary collision event. In case of high-Z materials such as Au there are many core electrons available with binding energies in the order of some 10 eV allowing for capture of several electrons during a single binary collision. This is not the case in Al and Si; the gap between the bottom of the conduction band and the least bound core electrons is 60 (Al) and 80 eV (Si). Therefore, the exchange mechanism proposed by Burgdörfer might be less effective in the case of these materials.

VI. DISCUSSION

In the previous sections we have tried to indicate the key factors that determine the overall shape of the KLL Auger spectra obtained from the interaction of hydrogenic nitrogen ions with solid surfaces. In the following we will discuss the features observed in the measured spectra using these general concepts.

The differences between the spectra arising from the Si(100) and the Al(110) target can be explained by two distinct L-shell filling mechanisms, via L Auger decay and by direct capture of target core electrons. The former process leads to L-shell filling rates in the order of 10^{13}/s up to $\simeq 10^{15}$/s with increasing number of L electrons r. This implies that for small r, i.e., at an early stage of the deexcitation when the projectile has not yet entered the close collision range, the KLL decay rate is much higher than the L Auger rate. This gives preferred decay as soon as the second L electron is present, yielding contributions to the low-energy side of the spectrum. The large L Auger rates only become effective when the projectile moves in the close collision range at or below the surface. The L Auger rates are independent of the projectile velocities used in the experiments under consideration here. However, they are dependent on the target specific electronic density. According to our model described above, the differences in peak intensities at the low-energy side of the spectra from Si and Al (Figs. 1 and 2) can be ascribed to different LVV filling rates. The electron density at the (p-doped) Si surface is orders of magnitude smaller than in case of the Al target, therefore, the associated Si L Auger rate is smaller than the Al counterpart, yielding a larger $P_K^\gamma(r = 2)$ for Si compared to Al. Similar "target effects" have been reported before, however for different experimental settings [23].

The second L-shell filling mechanism, direct capture of target core electrons, is localized and, therefore, dependent on the collision frequency, i.e., on the projectile velocity. As soon as the associated rate is larger than the KLL Auger rate, the L shell is rapidly filled up to its maximum shifting KLL energies to the higher values. The L-shell filling probability $P_L(r)$ [see Eq. (6)] might vary for different targets. But for large velocities ($v/d \gg \Gamma_K$) this variation will not be noticable since the L shell is filled up to its maximum before KLL decay occurs anyway. This explains why for large (16 keV) energies the high-energy side of the Si and Al spectra look alike (see Figs. 1 and 2). It should be noted that Köhrbrück *et al.* found support for a similar velocity dependent L-shell filling model by studying the angular distribution of the KLL Auger electrons [28].

The model presented in this paper allows one to estimate the spatial range s over which the initial potential energy of the projectile is released. According to this model, the largest part of this energy release, by emission of an energetic KLL Auger electron, takes place between the second and the nth binary collision in which n is the number of initial projectile L-shell vacancies. In practice this range is likely to be somewhat larger, depending on the probability $P_L(r)$ of the proposed capture process. Folkerts *et al.* [31] found an upper limit of 25 fs for the deexcitation of 60-keV O^{7+} on Au(110). Applying the L-filling model on this collision system gives a lower limit to the average probability to capture an L electron, $\overline{P}_L$ as follows: $7\overline{P}_L d/v \leq 25$ fs $\Rightarrow \overline{P}_L \geq 0.1$ (d/v equals the collision frequency mentioned before). A similar limit can be found using our data: for 16-keV N^{6+} ions at 2.5° incidence about 50 close collisions occur. Assuming complete neutralization (capture of 6-L electrons) afterwards this again gives a lower limit: $\overline{P}_L \geq 6/50 = 0.12$. So the proposed model nicely fits within the experimental boundary conditions.

Another interesting aspect of the consecutive filling of L vacancies by direct capture proposed here is that it implies the occurence of strong target lines in the Auger spectra. The shape of these target lines could resolve

the question of whether or not more than one electron is captured during each binary collision. This holds especially for low-Z targets such as Al and Si, since these materials do not contain core levels over a wide range of energies like high-Z metals such as Pt or Au. Therefore, single capture would lead to well-resolved, sharp target Auger lines whereas multiple capture during each collision would smear out the target line structure. A detailed study of target Auger emission is, in this context, of great interest.

VII. CONCLUSIONS

This paper presents a detailed discussion of the KLL Auger peak structure obtained from the interaction of hydrogenic N^{6+} ions with single crystal Al and Si surfaces. The exact shape of this structure appears to be the result of a intricate interplay of experimental parameters, part of which influence the actual physics of neutralization-deexcitation and part of which influence the extent to which the system can be observed.

Low projectile energies (i.e., E_0 in the order of tens to a few hundreds of eV) in conjuction with steep angles of incidence result in few close collisions. In this case both the density of weakly bound electrons at the surface and the work function influence the L-shell filling via Auger cascades. This is reflected in the dependence of the low-energy part of the KLL Auger spectrum on the specific target used.

Subsequent to this process, a direct filling of the L shell during consecutive close collisions becomes important, especially at higher collision energies. In this case, the filling rate is given by both the L Auger rates and the velocity dependent collision frequency.

The relative importance of these different filling mechanisms is reflected in both the target and the velocity dependence of the projectile K Auger spectra. Contributions from both above surface cascading and close collision filling can be distinguished.

ACKNOWLEDGMENTS

We gratefully acknowledge the excellent technical support given by Rob Kremers and Jans Sijbring. We would like to thank A. Arnau, J. Bleck-Neuhaus, R. Page, and R. Köhrbrück for stimulating discussions and their useful suggestions concerning this work. This work is part of the research program of the Stichting voor Fundamenteel Onderzoek der Materie (FOM) with financial support from the Nederlandse Organisatie voor Wetenschappelijk Onderzoek (NWO). Part of this work is sponsored by the EC program on Human Capital and Mobility, Grant No. ERBCHRXCT930103, and by the Bundesministerium für Forschung und Technologie.

[1] F. W. Meyer, S. H. Overbury, C. C. Havener, P. A. Zeijlmans van Emmichoven, and D. M. Zehner, Phys. Rev. Lett. **67**, 723 (1991).

[2] S. T. De Zwart, A. G. Drentje, A. L. Boers, and R. Morgenstern, Surf. Sci. **217**, 298 (1989).

[3] H. J. Andrä, A. Simionovici, T. Lamy, A. Brenac, G. Lamboley, J. J. Bonnet, A. Fleury, M. Bonnefoy, M. Chassevent, S. Andarimonje, and A. Pesnelle, Z. Phys. D **21**, S135 (1991).

[4] J. Burgdörfer, P. Lerner, and F. W. Meyer, Phys. Rev. A **44**, 5674 (1991).

[5] J. Das and R. Morgenstern, Phys. Rev. A **47**, R755 (1993).

[6] P. A. Zeijlmans van Emmichoven, C. C. Havener, and F. W. Meyer, Phys. Rev. A **43**, 1405 (1991).

[7] J. Das, L. Folkerts, and R. Morgenstern, Phys. Rev. A **45**, 4669 (1992).

[8] R. Köhrbrück, N. Stolterfoht, S. Schippers, S. Hustedt, W. Heiland, D. Lecler, J. Kemmler, and J. Bleck-Neuhaus, Phys. Rev. A **48**, 3731 (1993).

[9] S. Schippers, S. Hustedt, W. Heiland, R. Köhrbrück, J. Bleck-Neuhaus, J. Kemmler, D. Lecler, and N. Stolterfoht, Phys. Rev. A **46**, 4003 (1992).

[10] J. Bleck-Neuhaus, A. Saal, R. Page, P. Biermann, R. Köhrbrück, and N. Stolterfoht, Phys. Rev. A **49**, 1539 (1994); J. Bleck-Neuhaus, R. Page, and A. Saal, Nucl. Instrum. Methods Phys. Res. Sect. B **78**, 113 (1993).

[11] A. G. Drentje and J. Sijbring, Rev. Sci. Instrum. **63**, 2875 (1992).

[12] H. Niehus, W. Heiland, and E. Taglauer, Surf. Sci. Rep. **17**, 213 (1993).

[13] L. Folkerts, Ph.D. thesis, Rijksuniversiteit Groningen, 1992.

[14] H. Winter, Europhys. Lett. **18**, 207 (1992); H. Winter, C. Auth, R. Schuch, and E. Beebe, Phys. Rev. Lett. **71**, 1939 (1993).

[15] F. Aumayr, H. Kurz, D. Schneider, M. A. Briere, J. W. McDonald, C. E. Cunningham, and HP. Winter, Phys. Rev. Lett. **71**, 1943 (1993).

[16] H. Kurz, K. Töglhofer, HP. Winter, F. Aumayr, and R. Mann, Phys. Rev. Lett. **69**, 1140 (1993).

[17] S. Schippers, S. Hustedt, W. Heiland, R. Köhrbrück, J. Bleck-Neuhaus, J. Kemmler, D. Lecler, and N. Stolterfoht, Nucl. Instrum. Methods Phys. Res. Sect. B **78**, 106 (1993).

[18] M. T. Robinson and I. M. Torrens, Phys. Rev. B **9**, 5008 (1974); M. Hou and M. T. Robinson, Appl. Phys. **17**, 371 (1978).

[19] J. F. Ziegler, J. P. Biersack, and U. Littmark, in *Stopping Powers and Ranges of Ions in Matter*, edited by J. F. Ziegler (Pergamon, New York, 1985), p. 1.

[20] J. E. Hansen, O. Schraa, and N. Vaeck, Phys. Scr. **T41**, 41 (1992)

[21] S. Schippers, J. Limburg, J. Das, R. Hoekstra, and R. Morgenstern, Phys. Rev. A **50**, 540 (1994).

[22] R. D. Cowan, *The Theory of Atomic Structure and Spectra* (California University Press, Berkeley, 1981).

[23] J. Limburg, J. Das, S. Schippers, R. Hoekstra, and R.

Morgenstern, Surf. Sci. **313**, 355 (1994).
[24] J. Limburg, J. Das, S. Schippers, R. Hoekstra, and R. Morgenstern, Phys. Rev. Lett. **73**, 786 (1994).
[25] R. Díez Muiño, A. Arnau, and P. M. Echenique, Nucl. Instrum. Methods Phys. Res. Sect. B (to be published).
[26] N. Stolterfoht, Phys. Rep. **146**, 315 (1987), and references therein.
[27] L. Folkerts and R. Morgenstern, Europhys. Lett. **13**, 377 (1990); Z. Phys. D **21**, S351 (1991).
[28] R. Köhrbrück, M. Grether, A. Spieler, N. Stolterfoht, R. Page, A. Saal, and J. Bleck-Neuhaus, Phys. Rev. A **50**, 1429 (1994).
[29] R. Page, A. Saal, J. Thomaschewski, L. Aberle, J. Bleck-Neuhaus, R. Köhrbrück, M. Grether, and N. Stolterfoht (unpublished).
[30] J. Burgdörfer, C. Reinhold, and F. Meyer, Nucl. Instrum. Methods Phys. Res. Sect. B (to be published).
[31] L. Folkerts, S. Schippers, D. M. Zehner, and F. W. Meyer, Phys. Rev. Lett. **74**, 2204 (1995).